Article:
Miserev, D.S., Srinivasan, A., Tkachenko, O.A. et al. (2017) Mechanisms for Strong Anisotropy of In-Plane g-Factors in Hole Based Quantum Point Contacts. Physical Review Letters, 119 (11). 116803. ISSN: 0031-9007

https://doi.org/10.1103/PhysRevLett.119.116803

Mechanisms for Strong Anisotropy of In-Plane g-Factors in Hole Based Quantum Point Contacts

D. S. Miserev,[1] A. Srinivasan,[1] O. A. Tkachenko,[2] V. A. Tkachenko,[2,3] I. Farrer,[4] D. A. Ritchie,[5] A. R. Hamilton,[1] and O. P. Sushkov[1]

[1]School of Physics, University of New South Wales, Sydney 2033, Australia
[2]Rzhanov Institute of Semiconductor Physics of SB RAS, Novosibirsk 630090, Russia
[3]Novosibirsk State University, Novosibirsk 630090, Russia
[4]Department of Electronic and Electrical Engineering, University of Sheffield, Sheffield S10 2TN, United Kingdom
[5]Cavendish Laboratory, University of Cambridge, Cambridge CB3 0HE, United Kingdom

(Received 2 December 2016; revised manuscript received 2 March 2017; published 12 September 2017)

In-plane hole g factors measured in quantum point contacts based on p-type heterostructures strongly depend on the orientation of the magnetic field with respect to the electric current. This effect, first reported a decade ago and confirmed in a number of publications, has remained an open problem. In this work, we present systematic experimental studies to disentangle different mechanisms contributing to the effect and develop the theory which describes it successfully. We show that there is a new mechanism for the anisotropy related to the existence of an additional $B_+k_-^4\sigma_+$ effective Zeeman interaction for holes, which is kinematically different from the standard single Zeeman term $B_-k_-^2\sigma_+$ considered until now.

DOI: 10.1103/PhysRevLett.119.116803

A quantum point contact (QPC) is a narrow quasi-one-dimensional (1D) constriction linking two two-dimensional (2D) electron or hole reservoirs. Experimental studies of QPCs started with the discovery of the conductance quantization in steps of $G_0 = 2e^2/h$ [1,2]. The steps are due to the quantization of transverse channels [3]. Effects of many-body correlations in QPCs were identified by a "0.7-anomaly" in the conductance, an enhancement of the g factor in the 1D limit [4], and by a zero bias anomaly [5]. G factors in n-type QPCs have been measured in numerous experiments; a relatively recent one is reported in Ref. [6].

The in-plane electron g factor in a QPC takes the same value for any direction of the in-plane magnetic field. Even in InGaAs, which has appreciable spin-orbit coupling, no in-plane g-factor anisotropy has been observed [7]. Contrary to this, measurements for holes in QPCs based on GaAs p-type heterostructures indicate a huge anisotropy. All previously reported values of the g factor for magnetic fields applied perpendicular to the QPC are consistent with $g_\perp = 0$ within experimental error, while the g factor $g_{||}$ for the parallel direction is nonzero [8–10].

Regardless of numerous studies, the g-factor anisotropy effect in QPCs remains unclear. One mechanism to explain the g-factor anisotropy was suggested in Ref. [9]. This mechanism is based on the crystal anisotropy of the cubic lattice. While it is not negligible, the contribution of this mechanism is too small to explain the observed anisotropy.

In this work, we identify a new mechanism for the g-factor anisotropy unrelated to the crystal lattice. It is instructive to use classification in powers of crystal anisotropy η defined below. The new mechanism is leading in η and the mechanism [9] is subleading. The new mechanism is negligible at very low hole densities. However, at real physical densities it is the major anisotropy mechanism. Previous measurements were performed in 2D hole systems formed at a single heterojunction [8,9], which can be modeled as a triangular potential well. There is also a measurement with an asymmetric quantum well [10] which can be modeled as a square potential with an electric field along the z axis. The z axis is perpendicular to the plane of the 2D hole system. The z asymmetry results in the cubic Rashba spin orbit interaction (SOI) [11–14]. We will show that there are two major mechanisms for $g_\perp$ suppression, (i) the $g_1 - g_2$ mechanism, (ii) the Rashba mechanism. To disentangle the mechanisms, in the present work we perform measurements of QPC g factors for quantum well GaAs heterostructures which allows us to tune the Rashba SOI. By reducing the Rashba SOI we observe a nonzero $g_\perp$ for the first time (although the anisotropy is still large, with $g_{||} \gg g_\perp$). In all previous measurements the strong asymmetry of the heterostructure, or the high hole density, resulted in a very strong Rashba SOI, so both mechanisms contributed to suppression of $g_\perp$. The Rashba mechanism is not significant in our devices. (The mechanism is explained in the very end of the Letter and discussed in detail in the Supplemental Material D [15].) The hole gas is confined in a 15 nm rectangular quantum well. An external electric field E_z is superimposed on the well using an *in situ* back gate below the quantum well. The transconductance maps measured at $E_z = 1.2 \times 10^6$ V/m and $E_z = 2.5 \times 10^6$ V/m are presented in Figs. 1(a) and 1(b). The absolute values of the g factors extracted from these maps are shown in Fig. 1(c). All experimental details are provided in section A

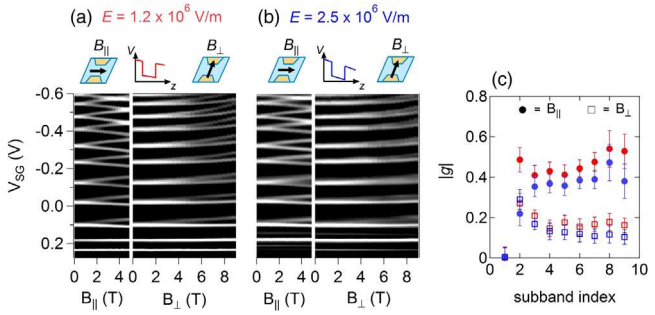

FIG. 1. Panels (a),(b): Grey-scale plots of the transconductance showing Zeeman spin splitting of 1D hole subbands in a magnetic field applied parallel and perpendicular the QPC. Panel a (Panel b) corresponds to the electric field along the z axis $E_z = 1.2\times10^6\,\mathrm{V/m}$ ($E_z = 2.5\times10^6$ V/m). Panel (c): Absolute values of the subband g factors extracted from data in panels (a) and (b). The circles (squares) correspond to the direction of magnetic field along (perpendicular) the QPC. The red (blue) symbols correspond to the out-of-plane electric field $E_z = 1.2\times10^6\,\mathrm{V/m}$ ($E_z = 2.5\times10^6$ V/m).

of the Supplemental Material [15], see also Refs. [16–18]. Figure 1 demonstrates a significant g-factor anisotropy. Another observation is that in all cases both g factors are very small for the lowest transverse channel, $n = 1$.

Dynamics of a single hole in bulk conventional semiconductors are described by the Luttinger Hamiltonian [19]. We consider here the spherical approximation [20]

$$H_L = \left(\gamma_1 + \frac{5}{2}\bar{\gamma}_2\right)\frac{\mathbf{p}^2}{2m} - \frac{\bar{\gamma}_2}{m}(\mathbf{p}\cdot\mathbf{S})^2, \qquad (1)$$

where $\mathbf{p}$ is the 3D quasimomentum; $\mathbf{S}$ is the spin $S = 3/2$; γ_1, $\bar{\gamma}_2 = (2\gamma_2 + 3\gamma_3)/5$ are Luttinger parameters; m is the free electron mass. There is also a nonspherical part of the Luttinger Hamiltonian that depends on the cubic lattice orientation. This part is proportional to $\eta = (\gamma_3 - \gamma_2)/\bar{\gamma}_2$. The parameter η is small in compounds with large SOI, for example $\eta = 0.34$ in GaAs and $\eta = 0.09$ in InAs. In Ref. [9] a mechanism of the QPC g-factor asymmetry due to the nonspherical part of the Luttinger Hamiltonian was suggested. The contribution of this mechanism is small and is calculated in section B of the Supplemental Material [15], see also Refs. [21–23]. Here we concentrate on the leading contribution which arises from the spherical Hamiltonian Eq. (1).

A quantum well potential $W(z)$ imposed on Eq. (1) confines dynamics along the z axis leading to 2D subbands. Here, we consider only the lowest subband with dispersion

$$H_0 = \varepsilon_{\boldsymbol{k}}, \qquad (2)$$

where $\boldsymbol{k} = (k_x, k_y) = (p_x, p_y)$ is the 2D momentum. At $k = 0$ the projection of spin on the z axis S_z is a good quantum number. Because of the negative sign of the second term in Eq. (1), the lowest band is a Kramers doublet with $S_z = \pm 3/2$. The standard way to describe the Kramers doublet is to introduce the effective spin $s = 1/2$ with related Pauli matrices $\boldsymbol{\sigma}$. The correspondence at $k = 0$ is very simple: $|\uparrow\rangle = |S_z = 3/2\rangle$, $|\downarrow\rangle = |S_z = -3/2\rangle$. Note that the effective spin operators $\sigma_\pm = \sigma_x \pm i\sigma_y$ flip $S_z = \pm 3/2$ projections. Hence, $\sigma_\pm$ are transformed as $S^3_\pm$.

Now we apply in-plane magnetic field $\mathbf{B}$. The kinematic structure of the effective 2D Zeeman Hamiltonian is of the form [21]

$$H_Z = -\frac{\mu_B}{4}\{\bar{g}_1[B_+k_+^2\sigma_- + B_-k_-^2\sigma_+] + \bar{g}_2[B_-k_+^4\sigma_- + B_+k_-^4\sigma_+]\}$$
$$g_1(k) = k^2\bar{g}_1(k), \qquad g_2(k) = k^4\bar{g}_2(k). \qquad (3)$$

Pauli matrices $\sigma_\pm$ ($\sigma_\pm^2 = 0$) have the angular momentum selection rule $\Delta J_z = \pm 3$, and $B_\pm$ corresponds to $\Delta J_z = \pm 1$. The powers of $k_\pm$ in Eq. (3) balance the z component of the angular momentum in such a way that the total Hamiltonian conserves the angular momentum, $\Delta J_z = 0$. While the g_1 term in Eq. (3) is well known, the g_2 term has never been considered before. In perturbative treatment of the Luttinger Hamiltonian Eq. (1), the g_2 term appears only in a high order of the perturbation theory. Of course, at small momenta $g_2 \ll g_1$, practically this is true if $kd < 0.6$, where d is the width of the well. However, all experiments we are aware of (including ours) are performed at $kd > 1.2$. In this case g_1 and g_2 are comparable.

The functions $g_1(k)$ and $g_2(k)$ have been calculated recently for symmetric heterostructures [21]. Here we calculate them for asymmetric ones. These functions for an infinite rectangular GaAs quantum well of width $d = 15$ nm with superimposed electric field E_z are plotted in Fig. 2(a).

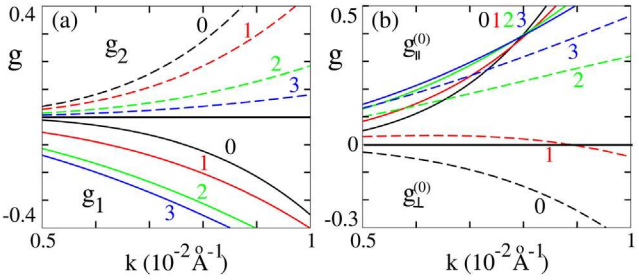

FIG. 2. Panel (a): Functions g_1 (solid lines) and g_2 (dashed lines) for the 2D system versus momentum, see Eqs. (3) and (8). Panel (b): Functions $g_{||}^{(0)}$ (solid lines) and $g_\perp^{(0)}$ (dashed lines) for the 1D system versus momentum, see Eqs. (4). Both panels are calculated for a rectangular GaAs quantum well of width $d = 15$ nm with a superimposed electric field E_z. We present plots for $E_z = 0$, 1, 2, 3 MV/m, with black, red, green, and blue lines, respectively. The value of the electric field in MV/m is pointed out near each line.

Remarkably the existence of two isotropic g functions leads to an anisotropy of the QPC g factor. The QPC g factor is determined experimentally by the splitting of the transconductance peaks in a magnetic field, see Fig. 1. We define the x axis to be along the QPC (the direction of the current) and the y axis perpendicular to the QPC. The transconductance peaks correspond to the chemical potential aligning with the 1D subband edges, where $k_x = 0$. Therefore, in the g-factor measurements $k = k_y$ and $k_\pm = \pm ik$. Hence, at the 1D subband edge the Zeeman interaction Eq. (3) for a QPC reads

$$H_Z \to -\frac{\mu_B}{2}\{g_{||}^{(0)} B_x \sigma_x + g_{\perp}^{(0)} B_y \sigma_y\}$$
$$g_{||}^{(0)}(k) = g_2(k) - g_1(k), \quad g_{\perp}^{(0)}(k) = -g_2(k) - g_1(k). \quad (4)$$

The superscript (0) indicates that these are terms of the zero order in η. Plots of $g_{||}^{(0)}(k)$ and $g_{\perp}^{(0)}(k)$ for an infinite 15 nm rectangular GaAs quantum well with different values of E_z are presented in Fig. 2(b).

Calculations of the in-plane Zeeman response have a nontrivial pitfall related to gauge invariance. This pitfall was overlooked in previous studies. To find the g functions we diagonalize the 3D Hamiltonian

$$H = H_L + W(z) - 2\kappa\mu_B \boldsymbol{B}\cdot\boldsymbol{S}$$
$$\boldsymbol{A} = [B_y(z - z_0), -B_x(z - z_0), 0], \quad (5)$$

where $\boldsymbol{A}$ is the vector potential included in H_L via "long derivatives" (for details see Ref. [21]), and 2κ is the bulk g factor. In Eq. (5) z_0 is an arbitrary constant. Because of gauge invariance, z_0 cannot affect any physical observable. However, at arbitrary z_0 the minimum of the 2D hole dispersion is generally not at $k = 0$. In particular, in this situation the transconductance peaks do not correspond to $k_x = 0$. To avoid this complication we fix the value of z_0 with the condition that the minimum of the dispersion is at $k_x = 0$. For a symmetric quantum well $W(z) = W(-z)$ the value of z_0 is dictated by symmetry, $z_0 = 0$, the center of symmetry of the well. In the next paragraph we discuss how to determine z_0 for an asymmetric heterostructure, $W(z) \neq W(-z)$.

An asymmetric quantum well gives rise to Rashba SOI

$$H_R = -\frac{i}{2}\alpha_k(k_+^3\sigma_- - k_-^3\sigma_+). \quad (6)$$

This term has to be added to the effective 2D Hamiltonian H_{2D} given by Eqs. (2) and (3). Besides the Rashba SOI Eq. (6) one more kinematic structure in the effective 2D Hamiltonian is possible,

$$H_B(\mathbf{k}) = \gamma_k([\mathbf{B}\times\mathbf{k}]\cdot\hat{\mathbf{z}}). \quad (7)$$

Here, γ_k is a momentum dependent coefficient. To the best of our knowledge, the term Eq. (7) was unknown in previous literature. The momentum independent part of γ_k can be gauged out, see below, hence $\gamma_k \propto k^2$ and H_B scales as k^3 similar to Eq. (6). According to our calculations, Eqs. (6) and (7) become comparable at $B \approx 10$ T. Note that Eqs. (6) and (7) are the only inversion asymmetric kinematic structures allowed by other symmetries in the effective 2D Hamiltonian in the spherical ($\gamma_3 = \gamma_2$) approximation. The term Eq. (7) can be absorbed in the dispersion, $\varepsilon_{\mathbf{k}} + H_B(\mathbf{k}) \approx \varepsilon_{\mathbf{k}+\mathbf{q}}$, where $\mathbf{q} = -m^*(k)\gamma_k[\mathbf{B}\times\hat{\mathbf{z}}]$ and $m^*(k) = k/(\partial\varepsilon_k/\partial k)$ is the effective mass. This shift is equivalent to the variation of z_0 discussed in the previous paragraph. To fix the dispersion minimum at $k = 0$ one needs to set $\gamma_{k=0} = 0$. The value of z_0 providing this condition follows from the equation

$$\left\langle \left(\frac{\partial H}{\partial \boldsymbol{k}}\right)_{\boldsymbol{k}=0} \right\rangle = \left.\frac{\partial H_{2D}}{\partial \boldsymbol{k}}\right|_{\boldsymbol{k}=0} = 0. \quad (8)$$

Here H is given by Eq. (5) and H_{2D} is the effective 2D Hamiltonian which includes terms Eqs. (2), (3), (6), and (7). Brackets stand for the averaging over the wave function corresponding to $k = 0$, but $B \neq 0$. Solving Eq. (8) in the linear in B approximation yields the value of z_0. The effect of quantum well asymmetry on the 2D functions $g_1(k)$, $g_2(k)$, and the 1D g factors $g_{||}^{(0)}(k)$ and $g_{\perp}^{(0)}(k)$ calculated with the constraint Eq. (8) for electric fields $E_z = 1$, 2, 3 MV/m are shown in Fig. 2 by the colored lines. The corresponding values of z_0 determined from Eq. (8) are $z_0(nm) = 1.38$, 2.37, 3.03 (zero is in the center of the square well).

To complete the discussion of gauge invariance, we would like to demonstrate that in the presence of the Rashba interaction Eq. (6) the functions g_1 and g_2 in Eq. (3) are not gauge invariant. Let us perform the shift gauge transformation $\boldsymbol{k} \to \boldsymbol{k} - \delta\boldsymbol{A}_0$, $\delta\boldsymbol{A}_0 = -\delta z_0[\boldsymbol{B}\times\hat{\mathbf{z}}]$. Hence the dispersion Eq. (2) is changed as $\varepsilon_k \to \varepsilon_{\boldsymbol{k}-\delta\boldsymbol{A}_0} \approx \varepsilon_k - (\partial\varepsilon_k/\partial\boldsymbol{k})\delta\boldsymbol{A}_0$. The $\delta\boldsymbol{A}_0$ term in this equation can be transferred to Eq. (7) leading to a change of $\gamma_k \to \gamma_k - \delta z_0/m^*$ that is discussed in the previous paragraph. One must also perform the shift of $\boldsymbol{k} \to \boldsymbol{k} - \delta\boldsymbol{A}_0$ in the Rashba interaction Eq. (6), $H_R(\boldsymbol{k}) \to H_R(\boldsymbol{k} - \delta\boldsymbol{A}_0) \approx H_R(\boldsymbol{k}) - (\partial H_R/\partial\boldsymbol{k})\delta\boldsymbol{A}_0$. The $\delta\boldsymbol{A}_0$ term in this equation can be transferred to Eq. (3), leading to the change $\mu_B\bar{g}_1 \to \mu_B\bar{g}_1 + \delta z_0(6\alpha_k + k\alpha_k')$, $\mu_B\bar{g}_2 \to \mu_B\bar{g}_2 - \delta z_0\alpha_k'/k$. Here $\alpha_k' = (\partial\alpha_k/\partial k)$ is the derivative of the Rashba coupling coefficient. Thus, the functions g_1 and g_2 are not gauge invariant. Of course, physical g factors are gauge invariant, but generally they are different from g_1, g_2. Only in the gauge fixed by Eq. (8) do the physical g factors coincide with g_1, g_2. The same is true for the subleading corrections $\bar{\delta}_1$ and $\bar{\delta}_2$ proposed in Ref. [9] and calculated in section B of the Supplemental Material [15].

Our experiments have been performed with a 2D hole density of 1.1×10^{11} cm^{-2}. It corresponds to a 2D Fermi momentum $k_F^{2D} = 0.83 \times 10^{-2}$ Å^{-1}. The QPC channel is defined by the "transverse" Hamiltonian, $H_{tr} = \varepsilon_k + U(y)$, $k = k_y$, where $U(y)$ is the transverse self-consistent potential of the QPC. The energy levels of this Hamiltonian E_n, enumerated by index $n = 1, 2, 3, \ldots$, correspond to the 1D transverse channels. Varying the split-gate voltage adjusts the self-consistent potential $U(y)$, providing the condition to depopulate the nth 1D subband, $E_n = \varepsilon_F$. This implies that $U(y)$ depends on n. The self-consistent potential $U(x, y)$ for our device is calculated in section C of the Supplemental Material [15] using the Thomas-Fermi-Poisson method, see Refs. [24–26]. The potentials $U(y) = U(x = 0, y)$ for $n = 1$, 3, 5, 8 are plotted in Fig. 3(a).

While for $n \geq 3$ the potential minimum in the 1D channel is practically zero, $U(0) \approx 0$, for $n = 1$ the value of $U(0)$ is large, just slightly smaller than the Fermi energy. Therefore, k_y in this case is much smaller than the Fermi momentum in the 2D reservoirs. Since the in-plane g factors scale roughly as k_y^2, the large value of $U(0)$ explains the very small values of g factors for $n = 1$, see Fig. 1(c). Note that the potentials in Fig. 3(a) are very close to those obtained a long time ago for electrons [27]. Note also that the behavior of g factors at $n = 2$ is different from that at $n \geq 3$ and from $n = 1$, see Fig. 1(c). This is because of two competing and comparable effects, (i) the reduction of g factors since $U(0) > 0$, (ii) the enhancement of g factors due to many body Coulomb interaction effects. The low n enhancement of the in-plane g factor due to many body effects is well known in electron systems [4]. Fortunately, both complications become irrelevant at $n \geq 3$. The condition $U(0) \approx 0$ holds, and the Coulomb interaction is sufficiently screened. The g factors at $n \geq 3$ can be determined from Fig. 2(b) by taking the values at $k = k_y = k_F^{2D}$.

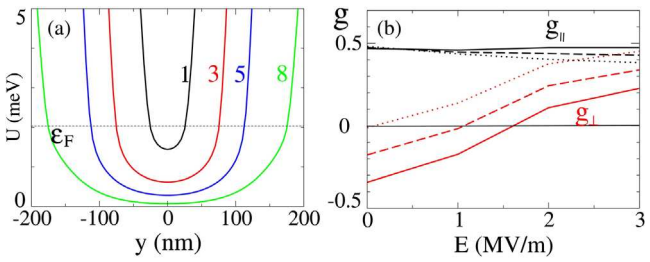

FIG. 3. (a) Self-consistent QPC transverse potential for 1D channels with $n = 1$, 3, 5, 8 subbands occupied. (b) QPC g factors $g_{\|}$ and $g_{\perp}$ for $n \geq 3$ versus electric field. The heterostructure is modeled as a 15 nm wide infinite rectangular quantum well with a superimposed electric field E_z. The hole density in the 2D leads is 1.1×10^{11} cm^{-2}. The dashed lines account only for the leading spherical contribution. The solid ([110] QPC orientation) and dotted ([100] QPC orientation) lines account for the leading contribution and for the first subleading one proportional to $\gamma_3 - \gamma_2$.

This gives the g factors $g_{\|}^{(0)}$ and $g_{\perp}^{(0)}$ shown by the dashed lines in Fig. 3(b), plotted versus the applied electric field.

To complete the story we have also taken into account the subleading η correction due to crystal anisotropy proposed in Ref. [9]. We have corrected the calculations of Ref. [9] for some errors as described in the Supplemental Material [15]. The η correction can be described by two momentum dependent functions $\delta_+(k)$ and $\delta_-(k)$ defined in section B of the Supplemental Material [15]. The η correction depends on the orientation of the QPC with respect to the crystal axes as given by Eq. (B7). In our experiment the QPC is oriented along the (110) direction; hence, the angle ϕ defined by Eq. (B5) is $\phi = \pi/4$. Therefore, according to Eq. (B7) $g_{\|} = g_{\|}^{(0)} - \delta_-$ and $g_{\perp} = g_{\perp}^{(0)} + \delta_+$. The plots of $\delta_{\pm}$ versus electric field are presented in panel B of Fig. B1 in the Supplemental Material [15]. Hence we arrive at the plots of $g_{\|}$ and $g_{\perp}$ versus electric field shown in Fig. 3(b) by the solid black and red lines. The calculated value of $g_{\|}$ is practically independent of the field, and is equal to $g_{\|} \approx 0.46$. In contrast, the perpendicular g factor $g_{\perp}$ depends on the field significantly, and even changes sign. However, at values of the field used in the experiment, $E_z = 1.2$ MeV/m and $E_z = 2.5$ MeV/m, the absolute values of the g factor are practically equal, $|g_{\perp}| \approx 0.17$. The theory agrees with data presented in Fig. 1. We stress that in $g_{\|}$ there is no compensation between different contributions; therefore, the calculation is rather reliable. On the other hand, for $g_{\perp}$ there is a significant compensation between the g_1 and g_2 contributions; therefore, the expected theoretical uncertainty in $g_{\perp}$ is larger than that in $g_{\|}$. Dotted lines in Fig. 3(b) show our prediction for the [100] orientation of the QPC. The essential ingredients of the theory are the functions $g_1(k)$, $g_2(k)$ considered in the main text and the coefficients $\delta_{\pm}$ calculated in the supplementary material. In principle, one can disentangle these parameters experimentally by performing measurements for different E_z with a set of QPCs aligned along different crystal orientations. Ideally the electric fields should encompass the values shown in Fig. 3(b), with QPC's oriented along the [110] and [100] directions. All the devices must have the same density of holes in leads.

Besides the $g_1 - g_2$ effect considered above, and the crystal anisotropy η correction calculated in section B of the Supplemental Material [15], there is one more effect influencing $g_{\perp}$. This 1D effect is due to a combination of the transverse QPC confinement with the Rashba SOI. It was previously addressed in numerical calculations for hole [28] and electron [29] wires. The 1D effect leads to $g_{\perp}$ oscillations and suppression with subband number n, $\propto (\sin \pi n \delta_R / \pi n \delta_R)$, where δ_R is a parameter related to the Rashba SOI. At the same time, $g_{\|}$ is not affected. This effect is weak in quantum wells, and hence is irrelevant for our experiments, but is relevant in other experiments [8–10].

The effect is discussed in section D of the Supplemental Material [15].

Conclusion.—We have performed systematic experimental and theoretical studies to resolve the problem of anisotropic g factors measured in quantum point contacts based on p-type heterostructures. We found that the most important mechanism for the anisotropy is related to the existence of two kinematically different effective Zeeman interactions for holes. Using our theory we make several predictions to motivate further experiments. The predictions include the effects of (i) Variation of density in the leads [Fig. 2(b)], (ii) Change of the QPC orientation [Fig. 3(b)], and (iii) Variation of the electric field E_z [Fig. 3(b)].

We thank Tommy Li and Stefano Chesi and Oleh Klochan for important discussions. The device used in this work was fabricated in part using facilities of the NSW Node of the Australian National Fabrication Facility. The work has been supported by the Australian Research Council Grants No. DP160100077 and No. DP160103630 and by the Russian Science Foundation Grant No. 14-22-00143.

[1] B. J. van Wees, H. van Houten, C. W. J. Beenakker, J. G. Williamson, L. P. Kouwenhoven, D. van der Marel, and C. T. Foxon, Phys. Rev. Lett. **60**, 848 (1988).
[2] D. A. Wharam, T. J. Thornton, R. Newbury, M. Pepper, H. Ahmed, J. E. F. Frost, D. G. Hasko, D. C. Peacock, D. A. Ritchie, and G. A. C. Jones, J. Phys. C **21**, L209 (1988).
[3] M. Büttiker, Phys. Rev. B **41**, 7906 (1990).
[4] K. J. Thomas, J. T. Nicholls, M. Y. Simmons, M. Pepper, D. R. Mace, and D. A. Ritchie, Phys. Rev. Lett. **77**, 135 (1996).
[5] S. M. Cronenwett, H. J. Lynch, D. Goldhaber-Gordon, L. P. Kouwenhoven, C. M. Marcus, K. Hirose, N. S. Wingreen, and V. Umansky, Phys. Rev. Lett. **88**, 226805 (2002).
[6] A. M. Burke, O. Klochan, I. Farrer, D. A. Ritchie, A. R. Hamilton, and A. P. Micolich, Nano Lett. **12**, 4495 (2012).
[7] T. P. Martin, A. Szorkovszky, A. P. Micolich, A. R. Hamilton, C. A. Marlow, R. P. Taylor, H. Linke, and H. Q. Xu, Phys. Rev. B **81**, 041303(R) (2010).
[8] J. C. H. Chen, O. Klochan, A. P. Micolich, A. R. Hamilton, T. P. Martin, L. H. Ho, U. Zülicke, D. Reuter, and A. D. Wieck, New J. Phys. **12**, 033043 (2010).
[9] Y. Komijani, M. Csontos, I. Shorubalko, U. Zülicke, T. Ihn, K. Ensslin, D. Reuter, and A. D. Wieck, Europhys. Lett. **102**, 37002 (2013).
[10] F. Nichele, S. Chesi, S. Hennel, A. Wittmann, C. Gerl, W. Wegscheider, D. Loss, T. Ihn, and K. Ensslin, Phys. Rev. Lett. **113**, 046801 (2014).
[11] Yu. A. Bychkov and E. I. Rashba, Sov. Phys. JETP Lett. **39**, 78 (1984).
[12] S. Chesi, G. F. Giuliani, L. P. Rokhinson, L. N. Pfeiffer, and K. W. West, Phys. Rev. Lett. **106**, 236601 (2011).
[13] R. Winkler, D. Culcer, S. J. Papadakis, B. Habib, and M. Shayegan, Semicond. Sci. Technol. **23**, 114017 (2008).
[14] F. Nichele, A. N. Pal, R. Winkler, C. Gerl, W. Wegscheider, T. Ihn, and K. Ensslin, Phys. Rev. B **89**, 081306(R) (2014).
[15] See Supplemental Material at http://link.aps.org/supplemental/10.1103/PhysRevLett.119.116803 for experimental details, crystal lattice corrections to the g-factor, electrostatics calculations of the device and the Rashba-induced suppression of the g-factor.
[16] W. R. Clarke, A. P. Micolich, A. R. Hamilton, M. Y. Simmons, K. Muraki, and Y. Hirayama, J. Appl. Phys. **99**, 023707 (2006).
[17] S. Birner, T. Zibold, T. Andlauer, T. Kubis, M. Sabathil, A. Trellakis, and P. Vogl, IEEE Trans. Electron Devices **54**, 2137 (2007).
[18] N. K. Patel, J. T. Nicholls, L. Martin-Moreno, M. Pepper, J. E. F. Frost, D. A. Ritchie, and G. A. C. Jones, Phys. Rev. B **44**, 13549 (1991).
[19] J. M. Luttinger, Phys. Rev. **102**, 1030 (1956).
[20] A. Baldereschi and N. O. Lipari, Phys. Rev. B **8**, 2697 (1973).
[21] D. S. Miserev and O. P. Sushkov, Phys. Rev. B **95**, 085431 (2017).
[22] G. E. Simion and Y. B. Lyanda-Geller, Phys. Rev. B **90**, 195410 (2014).
[23] X. Marie, T. Amand, P. Le Jeune, M. Paillard, P. Renucci, L. E. Golub, V. D. Dymnikov, and E. L. Ivchenko, Phys. Rev. B **60**, 5811 (1999).
[24] O. A. Tkachenko, V. A. Tkachenko, D. G. Baksheyev, K. S. Pyshkin, R. H. Harrell, E. H. Linfield, D. A. Ritchie, and C. J. B. Ford, J. Appl. Phys. **89**, 4993 (2001).
[25] J. A. Nixon, J. H. Davies, and H. U. Baranger, Phys. Rev. B **43**, 12638 (1991).
[26] O. A. Tkachenko, V. A. Tkachenko, Z. D. Kvon, A. V. Latyshev, and A. L. Aseev, Nanotechnologies in Russia, **5**, 676 (2010).
[27] S. E. Laux, D. J. Frank, and F. Stern, Surf. Sci. **196**, 101 (1988).
[28] M. M. Gelabert and L. Serra, Phys. Rev. B **84**, 075343 (2011).
[29] K. Kolasinski, A. Mrenca-Kolasinska, and B. Szafran, Phys. Rev. B **93**, 035304 (2016).